Aerosol and Air Quality Research, 18: 2519–2528, 2018

ISSN: 1680-8584 print / 2071-1409 online
doi: 10.4209/aaqr.2018.05.0166

Small Cyclones with Conical Contraction Bodies

Di Liu[1], Peng Wang[1], Ta-Chih Hsiao[2], Da-Ren Chen[1*]

[1] *Particle Laboratory, Department of Mechanical and Nuclear Engineering, Virginia Commonwealth University, Richmond, VA 23284, USA*
[2] *Graduate Institute of Environmental Engineering, National Central University, Taoyuan 32001, Taiwan*

ABSTRACT

The performance (i.e., cyclone pressure drop and particle penetration curve) of small cyclones with conical contraction bodies was investigated, with the cyclone used either as the size-selective inlet of a miniature/compact particle sensor/monitor or as a personal particle sampler. Prototype cyclones having inner bodies with conical contraction angles of 0°, 15° and 30° were constructed, and their performance was evaluated at various operational flow rates (viz., 1.0–7.0 L min^{-1}); the results indicate that a cyclone with a high body contraction angle is capable of collecting smaller particles than one with a low contraction angle at the same cyclone pressure drop. The effect of the vortex finder insertion length on the cyclone's performance was also studied and was found to be negligible. A linear relationship between the dimensionless particle cut-off size and the annular flow Reynolds number, Re_{ann} (in the log-log plot), could be found for the studied cyclones with characteristic cyclone velocity, calculated with the assumption of conservation of angular momentum for the swirling flow in a cyclone. Compared with previous studies, cyclones with conical contraction bodies have an advantage during lower pressure drops (up to 50%) for the same dimensionless particle cut-off size.

Keywords: Cyclone; Conical contraction body; Cyclone pressure drop; Cyclone particle cut-off size.

INTRODUCTION

Particulate matter (PM) is identified as one of the air pollutants worldwide. Epidemiologic studies have shown the adverse health effects of PM on human being (Ma *et al.*, 2011; Evans *et al.*, 2013; Samoli *et al.*, 2013; Pui *et al.*, 2014; Potera, 2014; Fan *et al.*, 2015). Cyclones have been widely applied to either recover or remove particulate matter (PM) in various industrial applications because of their simple design and low costs in manufacturing, operating and maintenance. Small/compact cyclones, operated at a low flow rate, are also designed as the PM samplers either for monitoring the personal exposure or as the size-selective inlet for particle sensors (Görner *et al.*, 2001; Lee *et al.*, 2010). Previous researches have been conducted to investigate the performance of small cyclones in various designs. Three low-flow cyclone families for personal PM sampling have been reported in the work of Kenny and Gussman (2000). Based on the study of Kenny and Gussman (2000), Cauda *et al.* (2014) evaluated two small cyclones with 1″ body diameter and used them as pre-selector for diesel particulate matter in mine environment. Hsiao *et al.* (2009) developed two miniature cyclones to remove particles with the sizes larger than 1.0 and 0.3 μm, respectively, at the operational flow rate of 0.3 L min^{-1}. A small quadru-inlet cyclone has also been developed to minimize the issue of directional sampling (Liu *et al.*, 2015). Sagot *et al.* (2017) studied a set of small cyclones and applied them to remove the oil mist in blow-by gases from combustion engines.

A majority of reported cyclones, socalled tangential-flow cyclones, have an inlet to tangentially introduce flow, a cylindrical body for flow swirling, a conical contraction (attached to the cylindrical body) for gathering all the collected particles together, and a vortex finder tube to vent the flow out (First, 1949; Kenny and Gussman, 1997; Hsiao *et al.*, 2015). The effect of the conical contraction on the performance of above cyclones (i.e., the cyclone pressure drop and particle cut-off size) has been reported in the literature. Kenny and Gussman (2000) have shown that the conical contraction part of a cyclone has an important impact on the cyclone performance. It was further concluded that the increase of the conical contraction part angle of a cyclone resulted in considerable increase in the cyclone pressure drop and reduction in the cyclone particle cut-off size (Xiang *et al.*, 2001; Avci and Karagoz, 2003).

As the flow swirls down the cylindrical body of a tangential-flow cyclone, the angular momentum of swirling flow decreases because of the presence of cylinder wall. The angular momentum of swirling flow is then increased

* Corresponding author.
E-mail address: dchen3@vcu.edu

once the flow enters the conical contraction part of a cyclone (because of the flow contraction). The contribution of a conical contraction part of a cyclone to the cyclone performance is thus believed being reduced with the presence of cylindrical body. It is therefore hypothesized that the maximal contribution of conical part on the cyclone performance, especially on the particle cut-off sizes, could be realized in the cases of a cyclone with conical contraction body (i.e., no cylindrical body). Indirect evidence has also been given in the work of Park *et al.* (2015), in which a three-stage cyclone separator (having a stepped contraction body instead of a cylindrical one) was studied.

To investigate the full potential of conical contraction on the performance of a tangential-flow cyclone, especially on the cyclone cut-off size, two small cyclones with conical contraction bodies were studied in this work. For the reference, a cyclone with the cylindrical body (having the same dimensions as those of studied ones) was also included in this work. Based on the experimental data, the semi-empirical models were further proposed to calculate the pressure drop and particle cut-off size of these studied cyclones.

STUDIED CYCLONES AND EXPERIMENTAL SETUP

Fig. 1 (i.e., the side and top cross-sectional views, Figs. 1(a) and 1(b), respectively) shows the schematic diagram of

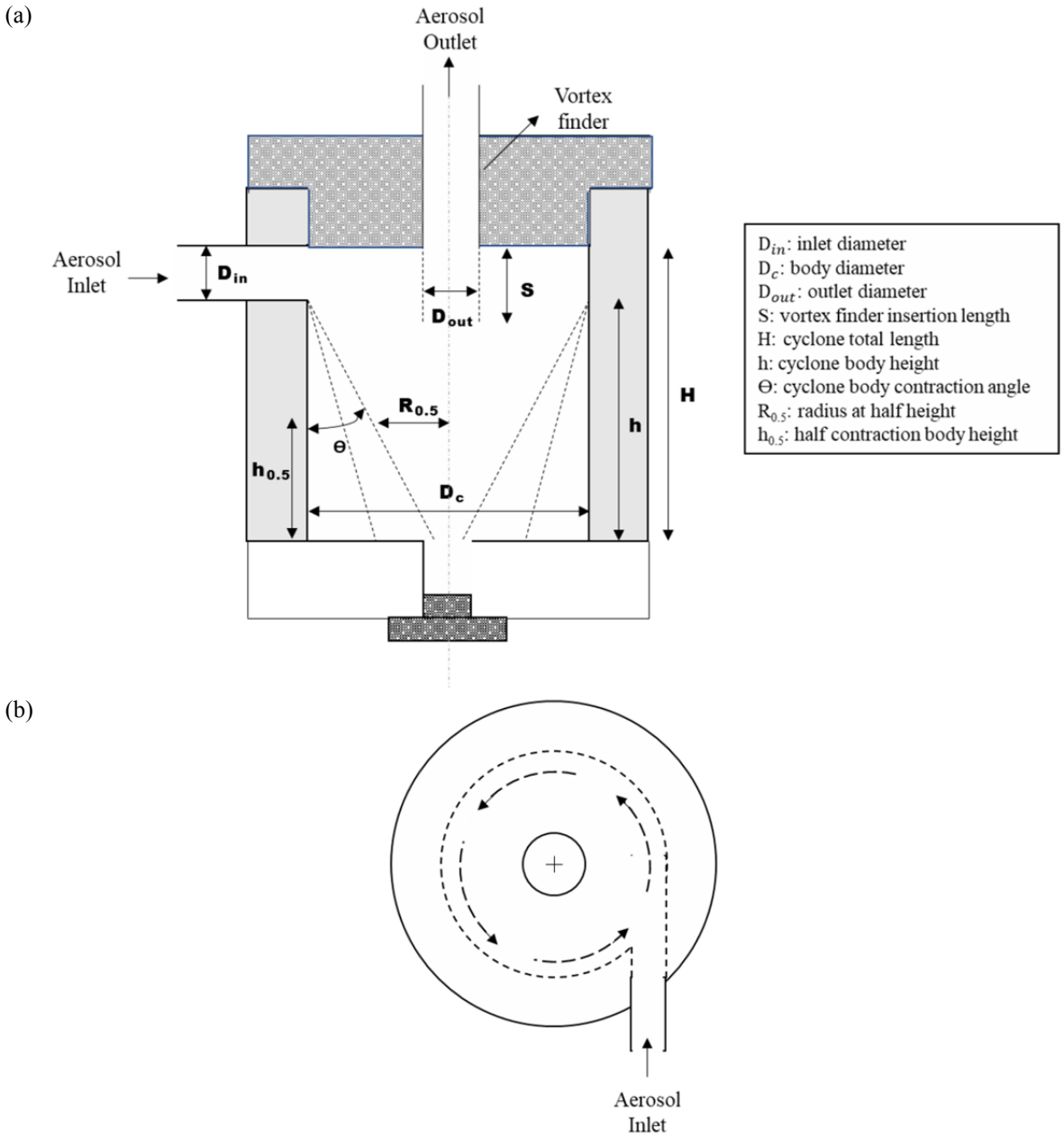

Fig. 1. Schematic diagram of studied cyclones with conical contraction body: (a) side cross-sectional view; (b) top cross-sectional view.

studied cyclones. The flow is tangentially introduced into the studied cyclones. A majority of key dimensions remains the same for all studied cyclones except the contraction angle, Θ, of cyclone body is varied (i.e., 0°, 15° and 30°). At the contraction angle, Θ, of zero, the studied cyclone is the same as the extra-sharp-cut cyclone (ESCC) studied by Kenny and Gussman (2000). The above cyclone was used as the reference. The other two cyclones have the conical contraction angles of 15° and 30°. Note that the conical contraction of cyclone body started right below the cyclone inlet in the above two cyclones (i.e., no cylindrical body section). A vortex finder (as the cyclone outlet) tube was installed at the cyclone cap. The overall size of these studied cyclones is comparable to the size of a U.S. quarter coin. Table 1 shows the key dimensions of the studied cyclones: the inlet diameter (D_{in}), the body diameter (D_c), the outlet diameter (D_{out}), the insertion length of the vortex finder (S), the cyclone total length (H), the cyclone body height (h) and the cyclone body contraction angle (Θ).

To characterize the performance of above cyclones, the cyclone pressure drop and particle penetration curve at different operational flow rates were measured. For the measurement of cyclone pressure drop, the operational flow was drawn from a cyclone via a vacuum pump and its rate was monitored by a laminar flow meter and controlled by a needle valve. Prior to the measurement, the laminar flowmeter was calibrated by the primary flow calibrator (Gilibrator-2, SENSIDYNE 800271). The pressure drop of a cyclone was measured by a differential pressure gauge (Series 2000, Magnehelic) with the high pressure end opened to the ambient.

Fig. 2 shows the schematic diagram of the experimental setup for the measurement of cyclone particle penetration curve. The studied cyclones were challenged by particles in a wide particle size range, i.e., 30 nm to 10 μm. Two sets of experimental setups were used for this part of evaluation: one is for sub-micrometer particle testing and the other is for super-micrometer particle testing. Particle generators and particle detectors were different in both setups.

The test chamber, installed vertically, was a cylindrical PVC pipe with 0.09 m in diameter and 1.5 m in height. A PVC cross connector was attached to the chamber top for introducing test particles from the top opening of the cross and filtered dilution flow from both side openings of the cross. The studied cyclone was placed near the bottom of the chamber. One channel of a three-way valve was connected to the cyclone and the other one was directly connected to a sampling tube for upstream particle measurement. By switching the valve channel, the particle size distributions at the upstream and downstream of the studied cyclones were measured. A vacuum pump was applied at the chamber bottom to vent the excess flow.

For the sub-micrometer particle testing, a custom-made Collison atomizer was used to generate polydisperse droplets containing KCl. Before being introduced into the test chamber, generated droplets were dried in a diffusion dryer with silica gel as the desiccant and charge-minimized by a radioactive Po^{210} neutralizer. The generated test particles have the mean size of 65 nm and with geometrical standard deviation $\sigma = 1.7 \pm 0.05$. The scanning mobility particle sizer (SMPS, TSI 3096) was used to measure the particle size distributions upstream and downstream of a studied cyclone. In the super-micrometer particle testing, the large particle generator (TSI 8108) was used to generate super-micrometer-sized KCL particles. In the large particle generator, testing particles were generated by spraying a KCl solution via a mechanical spray head and mixing with drying air carried with bipolar ions. An optical particle sizer (OPS, TSI 3330) was used to characterize the size distributions of super-micrometer-sized particles. The particle penetration curves of studied cyclones were obtained by taking the ratio of the particle concentration in each size bin at the cyclone downstream to that at the upstream.

Prototype cyclones were tested under five different flow rates (i.e., 1.0, 2.0, 3.0, 5.0 and 7.0 L min^{-1}). A makeup flow line with a HEPA filter cartridge, a laminar flow meter, a needle valve and a vacuum pump was included in the measurement line to ensure the operational flow rate of a studied cyclone.

RESULT AND DISCUSSION

On the Cyclone Pressure Drop

Fig. 3 shows the measured pressure drop of studied cyclones with three body contraction angles (i.e., 0°, 15° and 30°) as a function of the operational flow rate. The average inlet velocity of the cyclones is also given in the same plot. For each studied cyclone, we further varied the insertion length of the vortex finder tube (i.e., the ratio of S to H is 32%, 56% and 80%). It was found that the cyclone pressure drop varied with the cyclone body contraction angle. At the same operational flow rate, the cyclone with 30° body contraction angle had the highest pressure drop and one with the 0° body contraction angle had the lowest. The effect of vortex finder length on the cyclone pressure drop was found negligible for each tested cyclone under the same operational flow rate.

Similar to other small cyclones previously studied, the characteristic curves of cyclone pressure drop are in a quadratic form (as the function of inlet velocity). The loss

Table 1. Key dimensions for three studied cyclones.

Body Contraction Angle Θ (°)	Body Diameter D_c (inch)	Inlet Diameter D_{in} (inch)	Outer Diameter D_{out} (inch)	Vortex Finder Insertion Length S (inch)	Contraction Body Height h (inch)	Body Length H (inch)
0, 15 or 30	0.635*	0.125	0.068	0.2, 0.35 or 0.5*	0.5	0.625

* the ratio of D_c to H is around 1; the ratio of S to H for the three vortex finder insertion length are 32%, 56% and 80%, respectively.

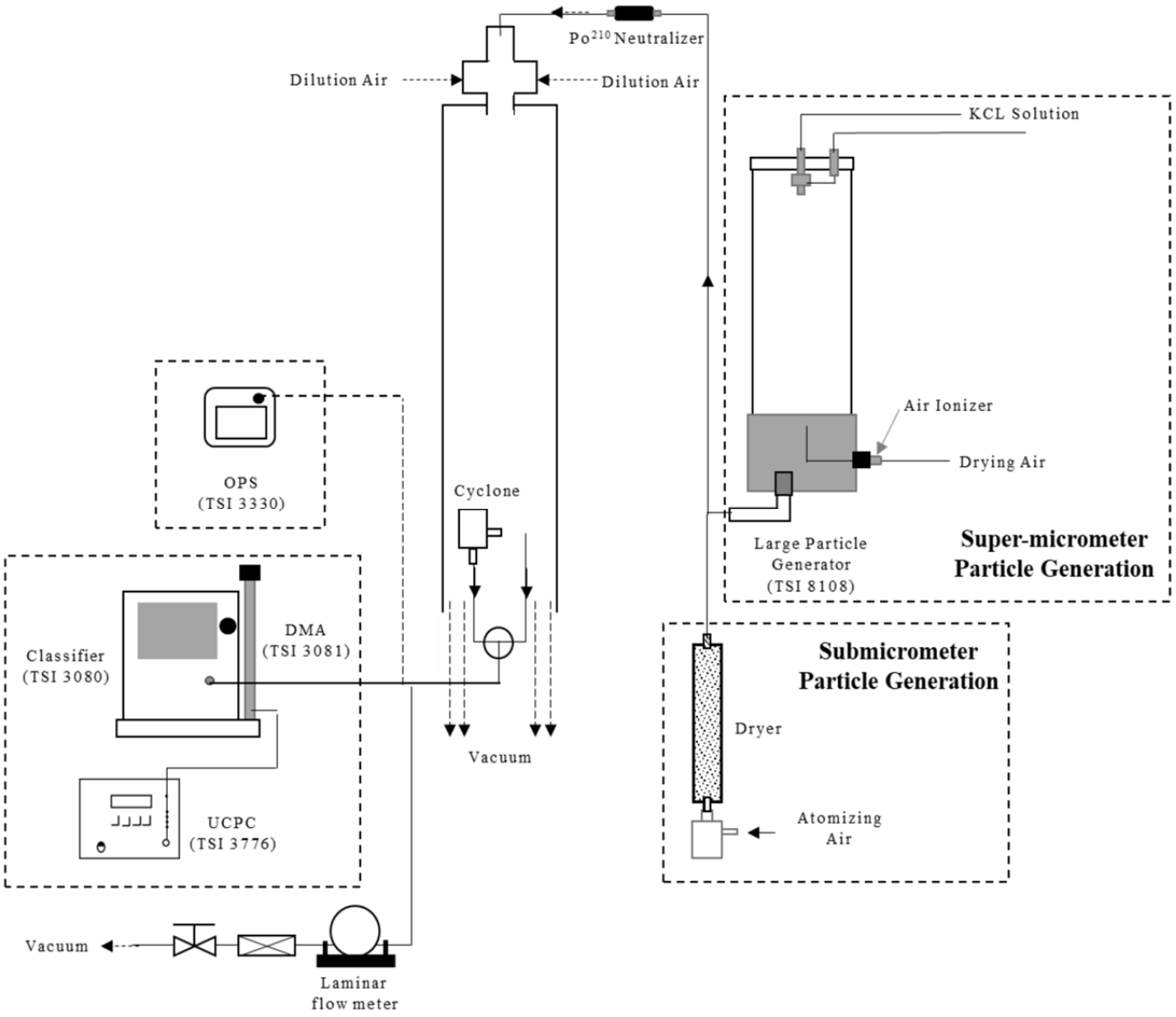

Fig. 2. Schematic diagram of experimental setups for measuring the particle penetration of prototype cyclones.

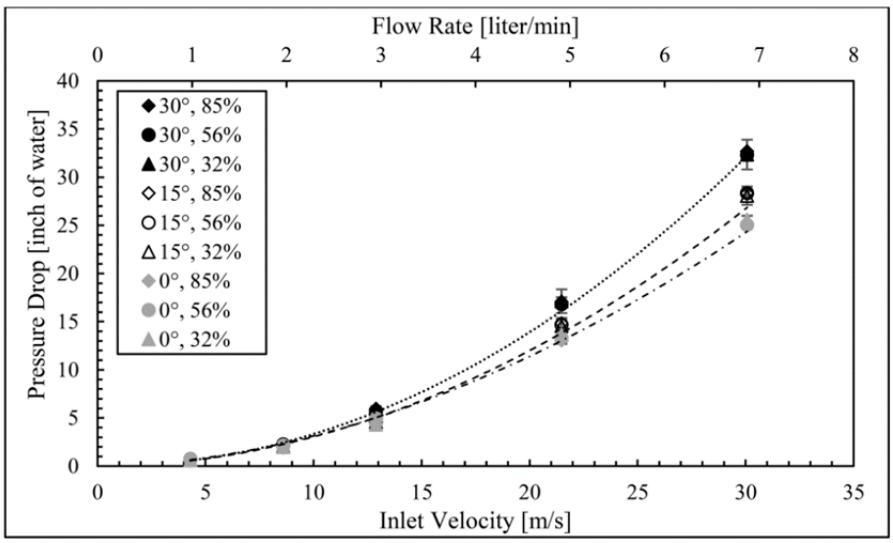

Fig. 3. Measured pressure drop as a function of cyclone inlet velocity of studied cyclones.

coefficient, K_L, defined as the ratio of measured pressure drop to the inlet dynamic pressure ($\rho_g V_i^2/2$), were 49.61, 55.59 and 62.17 for cyclones with 0°, 15° and 30° body contraction angles, respectively. Previous studies had proposed a semi-empirical model to predict the dimensionless loss coefficient (K_L) for the calculation of cyclone pressure drop. None of these models is for a small cyclone having a conical contraction body. Hsiao *et al.* (2009) successfully applied the Dirgo model (1988) to calculate the value of K_L for small cyclones with the cylindrical body. In this study, the Dirgo model again gave a reasonable prediction for the cyclone with the zero body contraction angle. However, the Dirgo model cannot be applied to the cases of cyclones with the body contraction angles of 15° and 30°, since they do not have the cylindrical part. A new semi-empirical model (based on the Dirgo's model) was thus proposed herein to calculate the value of K_L for small cyclones with conical contraction bodies. Instead of h, the difference between H and h (i.e., H-h) was used to avoid the mathematical singularity in Dirgo model. The new power index and coefficient were found by fitting the proposed equation to the experimental data. The working equations for the Dirgo and newly proposed models are shown in the following:

(1) Dirgo model

$$K_L = 19.7 \times \left(\frac{ab}{D_{out}^2}\right)^{0.99} \times \left(\frac{s}{D_c}\right)^{0.35} \times \left(\frac{H}{D_c^\circ}\right)^{-0.34} \times \left(\frac{h}{Dc}\right)^{-0.35} \times \left(\frac{B}{Dc}\right)^{-0.33} \quad (1)$$

(2) Proposed model

$$K_L = 17.81 \times \left(\frac{ab}{D_{out}^2}\right)^{0.99} \times \left(\frac{s}{D_c}\right)^{0.35} \times \left(\frac{H}{D_c^\circ}\right)^{-0.33} \times \left(\frac{H-h}{Dc}\right)^{-0.06} \times \left(\frac{B}{Dc}\right)^{-0.095} \quad (2)$$

where B is the diameter of cone bottom, which can be calculated from h, θ and D_c (i.e., $B = D_c - 2 \times h \times \tan\theta$). As shown in Fig. 4, the K_L values of the prototype cyclones can be reasonably estimated by the new proposed model. Note that the newly proposed model was also applicable to the cases of small cyclones studied by Hsiao *et al.* (2009) and quadru-inlet cyclones studied by Liu *et al.* (2015).

On the Particle Penetration Curves

Fig. 5 shows the particle penetration curves as the function of aerodynamic particle size for three studied cyclones operated at the flow rate of 3.0 liters per minute (L min^{-1}). Under the same operational flow rate, the particle cut-off size (defined as the particle size at the 50% penetration efficiency) of tested cyclones decreased with the increase of body contraction angles. The above observation further evidenced that the angular velocity of cyclone flow either remained the same or possibly increased as the flow swirled down the contraction body of a cyclone. The larger the contract angle, the stronger the swirl of the flow, resulting in the smaller particle cut-off size.

Fig. 6(a) gives the particle penetration curves as a function of dimensionless particle size for the cyclone with the 30° body contraction, operated at different flow rates (i.e., 1.0, 2.0, 3.0, 5.0 and 7.0 L min^{-1}). The dimensionless particle cut-off size is defined as $C^{0.5}D_p/D_c$, where C is the Cunningham correction factor; and D_p is the particle size. As the operational flow rate increased, the particle cut-off size of the studied cyclone decreased. For reference, the measured particle cut-off sizes for three studied cyclones at different operational flow rates are given in Table 2. The steepness of measured particle penetration curves for all these three cyclones under various annual Reynolds numbers, Re_{ann}, are shown in Fig. 6(b). Because of the conical contraction body of studied cyclones, we defined the annular flow Reynolds number of a cyclone as $Re_{ann} = (\rho \times V \times (D_c - D_{out}))/\mu$, where ρ and μ are the density and viscosity of carrier gas, respectively; and V is the characteristic velocity

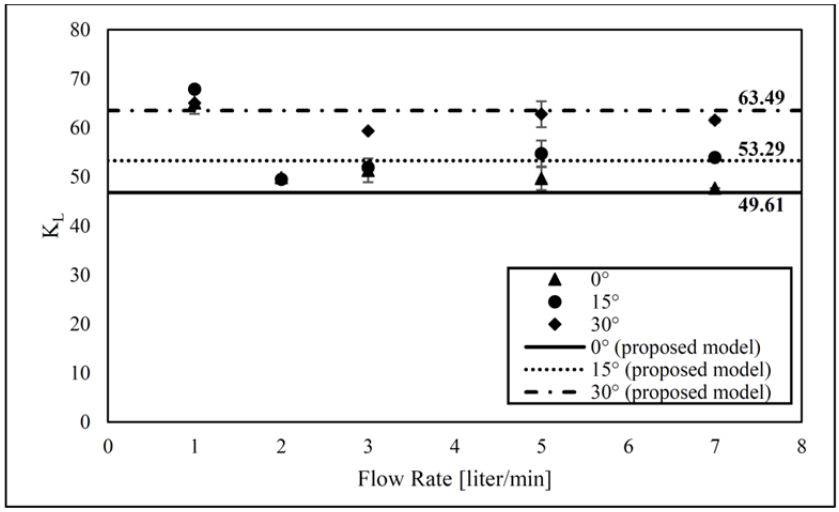

Fig. 4. The comparison of the measured and calculated loss coefficients (K_L) as a function of cyclone inlet velocity for the prototype cyclones (calculated by the revised Dirgo model).

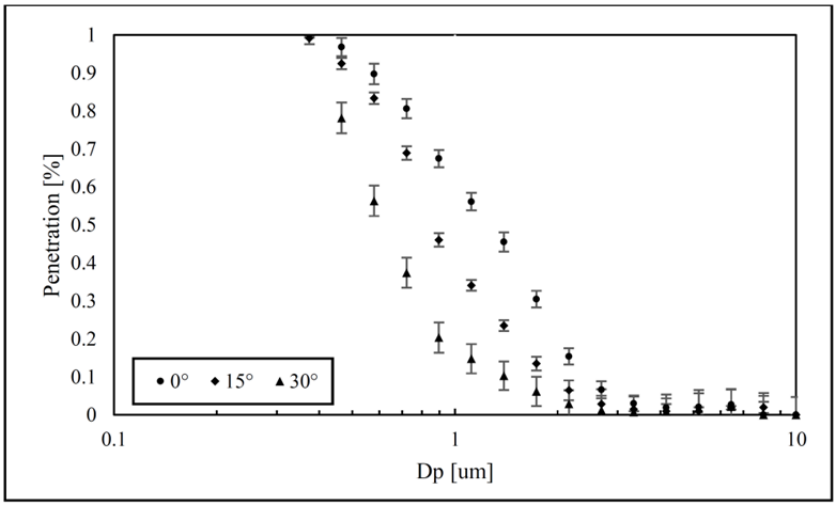

Fig. 5. The particle penetration as a function of aerodynamic particle size for prototype cyclones with different body contract angles (operated at 3.0 L min^{-1} flow rate).

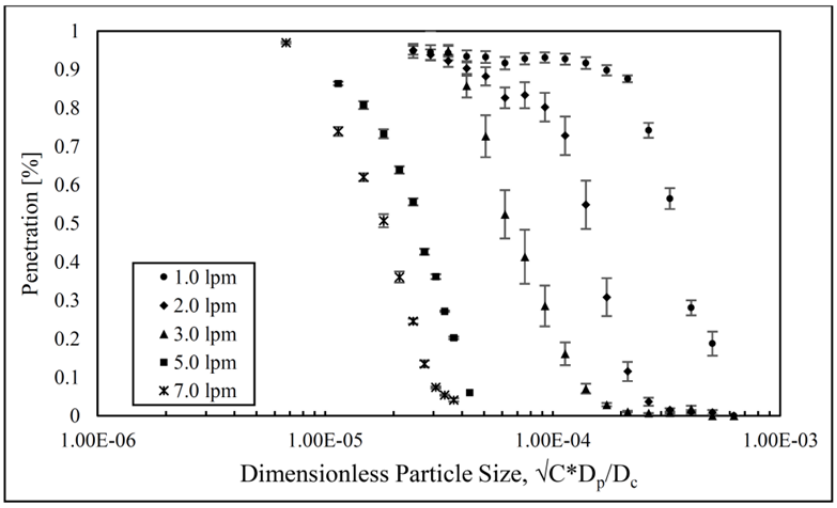

Fig. 6(a). The particle penetration as a function of dimensionless particle size for the cyclone with 30° contraction angle at different operational flow rates.

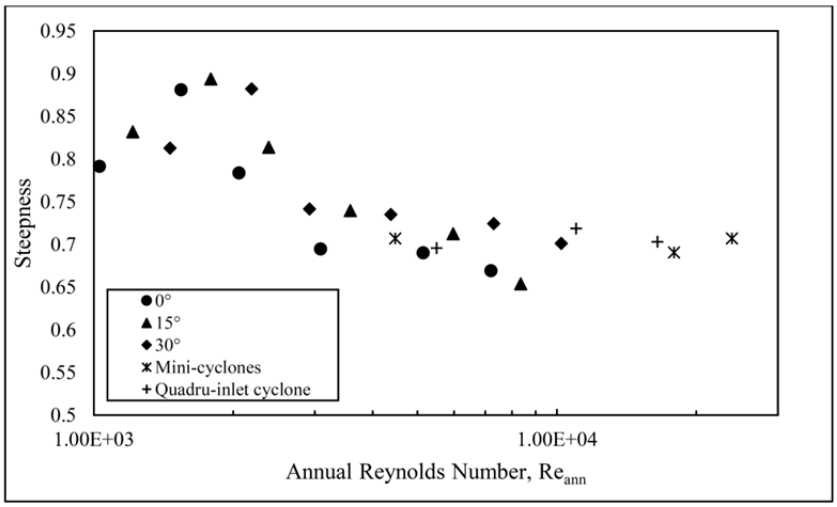

Fig. 6(b). The steepness of cyclone penetration curves as a function of cyclone flow rate for studied cyclones, mini-cyclones and quadru-inlet cyclone.

Table 2. Cut-off sizes for prototype tapered body cyclones under different flow rates.

Q [L min^{-1}]		1	1.5	2	3	5	7
$D_{p,50}$ [μm]	Θ = 0°	5.486	3.427	2.602	1.437	0.355	0.231
	Θ = 15°	5.470	3.555	2.263	0.944	0.320	0.204
	Θ = 30°	5.203	2.842	1.740	0.653	0.254	0.174

of tangential flow at the half height of the studied cyclone body, which is estimated as $V = (V_{in} \times R_c)/R_{0.5h}$ (where R_c is the cyclone body radius, V_{in} is the inlet velocity and $R_{0.5h}$ is the radius at half height of a cyclone). The steepness of the penetration curves was defined as the square root of the ratio of particle size at the 70% penetration efficiency to that at the 30% efficiency. The data of curve steepness for the mini-cyclones (Hsiao *et al.*, 2009) and the quadru-inlet cyclone (Liu *et al.*, 2015) are also included in Fig. 6(b). It is found that the steepness of particle penetration curves for the three studied cyclones first increased as the cyclone Reynolds number increased, decreased as the number exceeded 2,000, and then reached constant as the number exceeded 4,000. The above observation is possible because the effect of eddy motion in turbulent flow (in high Reynolds number regime) of a cyclone partially reduces the particle collection by the flow swirling. In general, the cyclones with the 15° and 30° body contraction angles offer slightly steeper cut-off curves as compared to the cyclones with a cylindrical body.

The effect of insertion length of the vortex finder tube on the performance of the studied cyclones was also investigated (S) while keeping the constant operational flow rate. Fig. 7 shows the measured particle penetration curves as a function of dimensionless particle size for the cyclone with the 30° body contraction angle and the vortex finder length of 0.2, 0.35 and 0.5 inches (i.e., the S/H ratios of 32%, 56% and 80%, respectively), when operated at the flow rate of 2.0 L min^{-1}. Negligible effect on the studied cyclone performance was found for the vortex finder insertion length. A similar observation was also found for the other two cyclones under different operational flow rates. The above result was consistent with the cyclone pressure drop shown in Fig. 3.

General Correlation

The linear relationship between the dimensionless particle cut-off size and the annular flow Reynolds number in the log-log plot (i.e., $\log((C^{0.5}D_{p,50})/D_c) = a + b \times \log Re_{ann}$) has been reported in the work of Moore and McFarland (1990). Fig. 8 shows the dimensionless particle cut-off size ($C^{0.5}D_{p,50})/D_c$) as a function of the annular flow Reynolds number (Re_{ann}). The dimensionless particle cut-off size is defined as $C^{0.5}D_{p,50}/D_c$, where $D_{p,50}$ is the particle cut-off size at the 50% particle penetration efficiency. Under the proposed definition of Re_{ann}, the linear relationship between the dimensionless particle cut-off size and Re_{ann} was again observed in the log-log plot for studied cyclones. It is also evidenced that as the annular flow Reynolds number increased, the dimensionless particle cut-off size decreased. A linear regression of the above data for the studied cyclones was also given in Fig. 8. The slope and the interception constant of the linear equation are –1.5953 and 1.4878, respectively. The given regression equation can be applied for the future design of small cyclones with conical contraction body. The data and associated regression for mini-cyclones and quadru-inlet cyclone were also included in Fig. 8. In comparison, the highest slope of linear regression was observed in the cases of cyclones with conical contraction body and the lowest slope of linear regression occurred in the cases of mini-cyclones. The above observation indicates that, at the same Re_{ann}, studied cyclones would have the

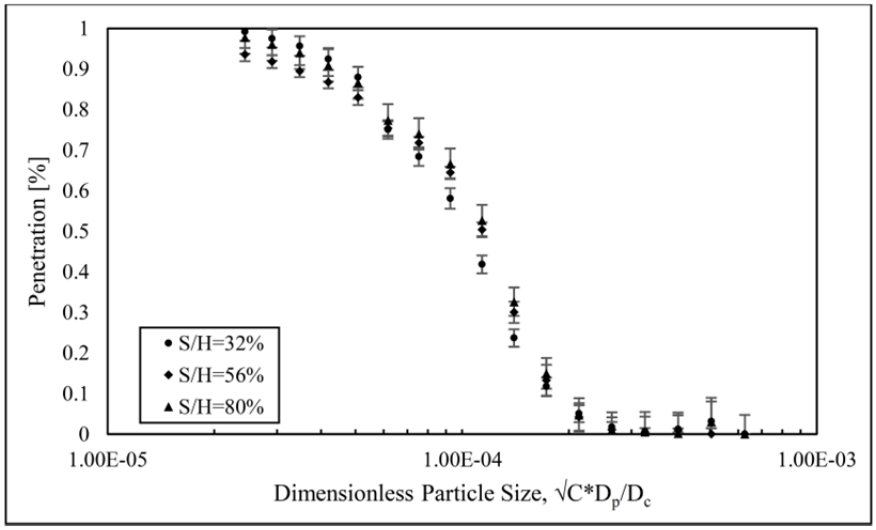

Fig. 7. The particle penetration as a function of dimensionless particle size for prototype cyclones having different insertion length of vortex finder tube.

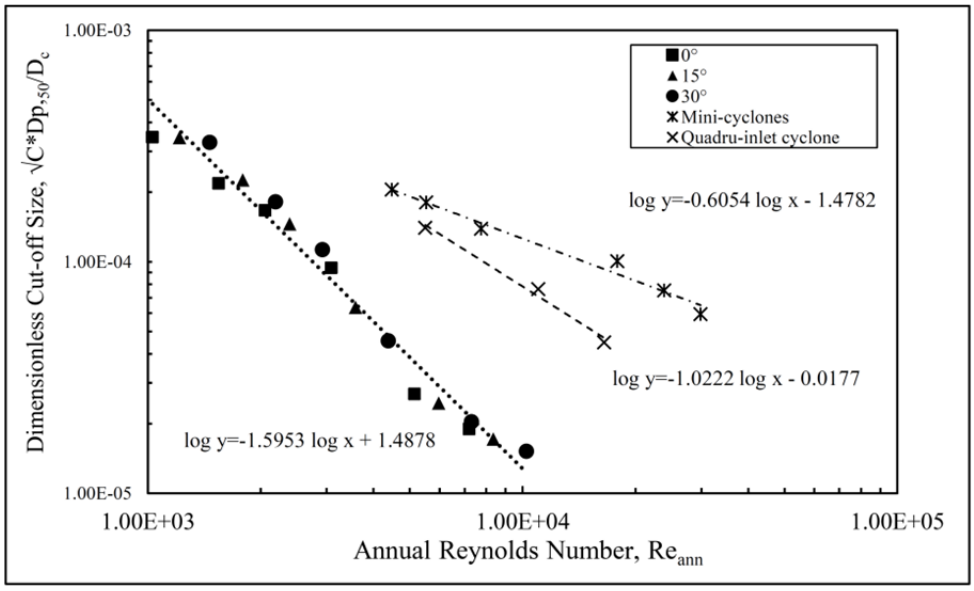

Fig. 8. The correlation of dimensionless particle cut-off size to annular flow Reynolds number for studied cyclones. The correlations for mini-cyclone and quadru-inlet cyclone are also included.

smallest dimensionless cut-off sizes among all compared cyclones. Further analysis shows that the ratio of cyclone body height (H) to cyclone flow inlet diameter (i.e., D_{in}) has significant correlation with the slope of linear regression (i.e., the lower the ratio, the steeper the slope). The low D_{in}/H ratio, which implies a low number of flow swirling turns in a cyclone, resulted in less frictional loss on the angular momentum of swirling flow. The other possible reason for the above observation might be due to the fact that it is easier to achieve the flow injection perfectly tangential to the cyclone body wall in studied cyclones than that in the other cyclones. It is because of much smaller flow opening designed in the mini- and quadru-inlet cyclones (when compared with that of studied cyclones).

The correlation between the dimensionless particle cut-off sizes and the pressure drop of the studied cyclones is also given in Fig. 9. For the comparison, we also included the data for mini-cyclones and quadru-inlet cyclones in the above figure. The "one-to-one" relationship between the dimensionless particle cut-off sizes and the pressure drop was obtained for each cyclone. In general, the dimensionless particle cut-off size of a cyclone decreased as the cyclone pressure drop increased. For studied cyclones, a rapid decrease in the particle cut-off size was observed as the cyclone pressure drop increased and less than 10 in H_2O (at which the operational flow rate was less than 3.0 L min^{-1}). The decrease in the cut-off size became gradual as the cyclone pressure drop further increased. To gain the maximal reward in the cut-off size reduction per unit pressure-drop increase, studied cyclones should be operated at a flow rate less than 3.0 L min^{-1}. It is because the power consumption required for cyclone operation is directly proportional to the cyclone pressure drop. More, for the same dimensionless particle cut-off size, the studied cyclone with large body contraction has lower pressure drop than the studied cyclone with cylindrical body. The maximal difference on the cyclone pressure drop could be up to 50%.

CONCLUSION

The performance (i.e., the cyclone pressure drop and the particle penetration curve) of small cyclones with conical contraction bodies (15° and 30°) was investigated in this study. As a reference, a cyclone with a cylindrical body (of the same dimensions) was also included. The performance evaluation was performed at different operational flow rates. In addition, the effect of the vortex finder insertion length was investigated.

According to the experimental results, the cyclone pressure drop for all three studied cyclones increased (in the form of a polynomial of the 2nd order) as the cyclone inlet velocity increased. The loss coefficient, K_L, for the cyclones was obtained. Our study found that the conical contraction of the cyclone body had an obvious effect on the cyclone pressure drop: the larger the contraction, the higher the pressure drop. However, the effect of the vortex finder insertion length on the pressure drop was negligible at the same operational flow rate. An empirical model was also proposed to calculate the pressure drop of the studied cyclones.

At the same operational flow rate, a cyclone with a larger body contraction (i.e., 30°) offers a smaller particle cut-off size compared to small cyclones with less contraction (i.e., 0° and 15°). For each studied cyclone, the increase in operational flow rate resulted in a decrease in the particle cut-off size (due to the increase in centrifugal force). A minor effect from the vortex finder insertion length on the cyclone particle cut-off size was also found. Using the revised characteristic velocity, a linear relationship between the dimensionless particle cut-off size and the annular flow Reynolds number was observed in the log-log plot for all studied cyclones. This general correlation can be applied to

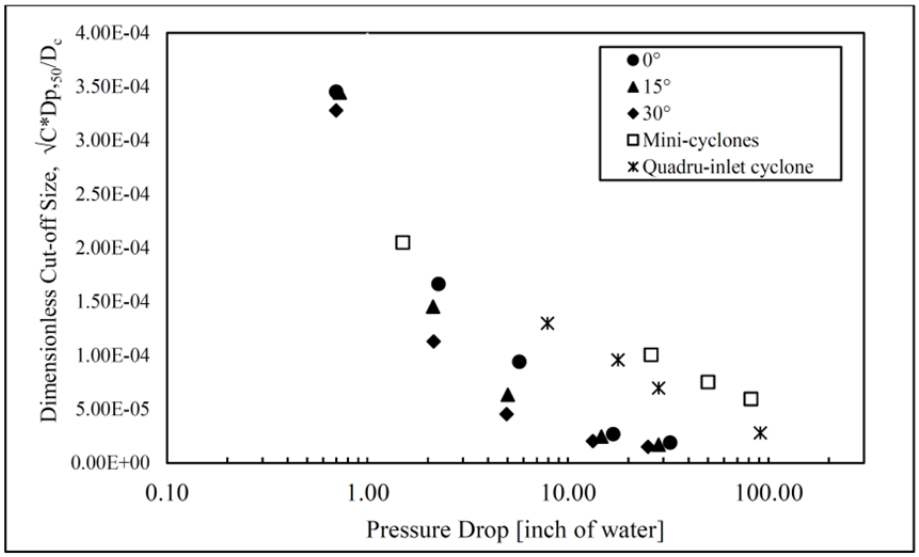

Fig. 9. The correlation between dimensionless cut-off size and cyclone pressure drop for studied cyclones, mini-cyclone and quadru-inlet cyclone.

the design of small cyclones with a conical contraction body. The relationship between the dimensionless particle cut-off size and the pressure drop of the studied cyclones was also identified. In cases with an identical cyclone pressure drop, the cyclone with a larger body contraction angle removes smaller particles as compared to cyclones with a smaller contraction angle.

REFERENCE

Avci, A. and Karagoz, I. (2003). Effects of flow and geometrical parameters on the collection efficiency in cyclone separators. *J. Aerosol Sci.* 34: 937–955.

Cauda, E., Sheehan, M., Gussman, R., Kenny, L. and Volkwein, J. (2014). An evaluation of sharp cut cyclones for sampling diesel particulate matter aerosol in the presence of respirable dust. *Ann. Occup. Hyg.* 58: 995–1005.

Dirgo, J. (1988). *Relationships between cyclone dimensions and performance*. Ph.D. thesis, Harvard University, Cambridge, MA, USA.

Evans, J., van Donkelaar, A., Martin, R.V., Burnett, R., Rainham, D.G., Birkett, N.J. and Krewski, D. (2013). Estimates of global mortality attributable to particulate air pollution using satellite imagery. *Environ. Res.* 120: 33–42.

Fan, J., Li, S., Fan, C., Bai, Z. and Yang, K. (2016). The impact of $PM_{2.5}$ on asthma emergency department visits: A systematic review and meta-analysis. *Environ. Sci. Pollut. Res.* 23: 843–850.

First, M. (1949). Cyclone dust collector design. *Am. Soc. Mech. Eng.* 49: 127–132.

Görner, P., Wrobel, R., Micka, V., Skoda, V., Denis, J. and Fabriès, J.F. (2001). Study of fifteen respirable aerosol samplers used in occupational hygiene. *Ann. Occup. Hyg.* 45: 43–54.

Hsiao, T.C., Chen, D.R. and Son, S.Y. (2009). Development of mini-cyclones as the size-selective inlet of miniature particle detectors. *J. Aerosol Sci.* 40: 481–491.

Hsiao, T.C., Huang, S.H., Hsu, C.W., Chen, C.C. and Chang, P.K. (2015). Effects of the geometric configuration on cyclone performance. *J. Aerosol Sci.* 86: 1–12.

Kenny, L.C. and Gussman, R.A. (1997). Characterization and modelling of a family of cyclone aerosol preseparators. *J. Aerosol Sci.* 28: 677–688.

Kenny, L.C. and Gussman, R.A. (2000). A direct approach to the design of cyclones for aerosol-monitoring applications. *J. Aerosol Sci.* 31: 1407–1420.

Kenny, L.C., Gussman, R. and Meyer, M. (2000). Development of a sharp-cut cyclone for ambient aerosol monitoring applications. *Aerosol Sci. Technol.* 32: 338–358.

Lee, T., Kim, S.W., Chisholm, W.P., Slaven, J. and Harper, M. (2010). Performance of high flow rate samplers for respirable particle collection. *Ann. Occup. Hyg.* 54: 697–709.

Lidén, G. and Gudmundsson, A. (1997). Semi-empirical modelling to generalise the dependence of cyclone collection efficiency on operating conditions and cyclone design. *J. Aerosol Sci.* 28: 853–874.

Liu, D., Hsiao, T.C. and Chen, D.R. (2015). Performance study of a miniature quadru-inlet cyclone. *J. Aerosol Sci.* 90: 161–168.

Ma, Y., Chen, R., Pan, G., Xu, X., Song, W., Chen, B. and Kan, H. (2011). Fine particulate air pollution and daily mortality in Shenyang, China. *Sci. Total Environ.* 409: 2473–2477.

Moore, M.E. and McFarland, A.R. (1990). Design of stairmand-type sampling cyclones. *Am. Ind. Hyg. Assoc. J.* 51: 151–159.

Park, C.W., Song, D.H. and Yook, S.J. (2015). Development of a single cyclone separator with three stages for size-selective sampling of particles. *J. Aerosol Sci.* 89: 18–25.

Potera, C. (2014). Toxicity beyond the Lung: Connecting $PM_{2.5}$, Inflammation, and Diabetes. *Environ. Health Perspect*. 122: A29–A29.

Pui, D.Y.H., Chen, S.C. and Zuo, Z. (2014). $PM_{2.5}$ in China: Measurements, sources, visibility and health effects, and mitigation. *Particuology* 13: 1–26.

Sagot, B., Forthomme, A., Yahia, L.A.A. and De La Bourdonnaye, G. (2017). Experimental study of cyclone performance for blow-by gas cleaning applications. *J. Aerosol Sci.* 110: 53–69.

Samoli, E., Stafoggia, M., Rodopoulou, S., Ostro, B., Declercq, C., Alessandrini, E., Díaz, J., Karanasiou, A., Kelessis Apostolos, G., Le Tertre, A., Pandolfi, P., Randi, G., Scarinzi, C., Zauli-Sajani, S., Katsouyanni, K. and Forastiere, F. (2013). Associations between fine and coarse particles and mortality in Mediterranean cities: Results from the MED-PARTICLES project. *Environ. Health Perspect*. 121: 932–938.

Xiang, R., Park, S.H. and Lee, K.W. (2001). Effects of cone dimension on cyclone performance. *J. Aerosol Sci.* 32: 549–561.

Received for review, May 17, 2018
Revised, July 27, 2018
Accepted, July 30, 2018